Published on 22 December 2015. Downloaded by Academia Sinica - Taipei on 22/01/2016 05:06:09.

Nanoscale

PAPER

View Article Online
View Journal | View Issue

Cite this: *Nanoscale*, 2016, **8**, 2284

High photosensitivity and broad spectral response of multi-layered germanium sulfide transistors†

Rajesh Kumar Ulaganathan,[a,b,c] Yi-Ying Lu,[a,b] Chia-Jung Kuo,[a,b] Srinivasa Reddy Tamalampudi,[b,c,d] Raman Sankar,[e] Karunakara Moorthy Boopathi,[c,f] Ankur Anand,[b,c,f] Kanchan Yadav,[a,b,c] Roshan Jesus Mathew,[b,c,f] Chia-Rung Liu,[a,b] Fang Cheng Chou[e] and Yit-Tsong Chen*[a,b]

Received 1st September 2015,
Accepted 18th December 2015

DOI: 10.1039/c5nr05988g

www.rsc.org/nanoscale

In this paper, we report the optoelectronic properties of multi-layered GeS nanosheet (~28 nm thick)-based field-effect transistors (called GeS-FETs). The multi-layered GeS-FETs exhibit remarkably high photoresponsivity of $R_\lambda \sim 206$ A W^{-1} under 1.5 μW cm^{-2} illumination at λ = 633 nm, V_g = 0 V, and V_{ds} = 10 V. The obtained $R_\lambda \sim 206$ A W^{-1} is excellent as compared with a GeS nanoribbon-based and the other family members of group IV–VI-based photodetectors in the layered-materials realm, such as GeSe and SnS_2. The gate-dependent photoresponsivity of GeS-FETs was further measured to be able to reach $R_\lambda \sim$ 655 A W^{-1} operated at V_g = −80 V. Moreover, the multi-layered GeS photodetector holds high external quantum efficiency (EQE ~ 4.0 × 10^4%) and specific detectivity ($D^* \sim 2.35 \times 10^{13}$ Jones). The measured D^* is comparable to those of the advanced commercial Si- and InGaAs-based photodiodes. The GeS photodetector also shows an excellent long-term photoswitching stability over a long period of operation (>1 h). These extraordinary properties of high photocurrent generation, broad spectral range, and long-term stability make the GeS-FET photodetector a highly qualified candidate for future optoelectronic applications.

Introduction

Layered materials are attractive building blocks in the modern electronic world. The exploration of such novel layered structures is especially interesting in optoelectronics for applications such as in transistors, photodetectors, ultrafast lasers, touch panels, and optical modulators to achieve the ever increasing demands for high-speed performance, less-power consumption, and easy-to-fabricate flexible devices.[1–4] Compared with zero- and one-dimensional materials, by virtue of their excellent electron mobility and large surface area, two-dimensional (2D) materials are well suited for easy integration into the complex electronic circuitry that pervades the modern electronics industry.[5,6]

The discovery of graphene has ignited tremendous development in materials science because of its unique, novel, and exciting electrical and mechanical properties. However, the absence of a band gap and weak light absorption in graphene limit its advantageous optoelectronic applications, therefore paving the way for other 2D layered semiconducting materials with versatile electronic and optical applications. To date, various layered materials, such as transition metal dichalcogenides (*e.g.*, MoS_2,[7] $MoSe_2$,[8] WS_2,[9] and $MoTe_2$[10]) and other multi-layered 2D crystals (*e.g.*, GaS,[11] GaSe,[12] and InSe[13]) have attracted significant attention and have been investigated. In particular, the layered chalcogenides of group IV–VI (GeS,[14] GeSe,[15] SnS,[16] SnSe,[17] *etc.*) have attracted wide research interest because of their suitable band gaps, high absorption coefficients, anisotropic optical/electrical properties, high thermal stability, low toxicity, and environmental sustainability. For example, single-crystal germanium selenide (GeSe) nanosheet-based photodetectors were demonstrated to possess excellent photoresponsivity ($R_\lambda \sim 3.5$ A W^{-1}) and photoconductive gain (~5.3 × 10^2%).[18] These encouraging results motivated us to investigate the photoresponsive properties of germanium sulfide (GeS), which have not been explored elaborately so far, despite the band gap of GeS lying in the convenient visible

[a]Department of Chemistry, National Taiwan University, Taipei 10617, Taiwan. E-mail: ytcchem@ntu.edu.tw
[b]Institute of Atomic and Molecular Sciences, Academia Sinica, Taipei 10617, Taiwan
[c]Nano Science and Technology Program and Molecular Science and Technology Program, Taiwan International Graduate Program, Academia Sinica, Nankang 11529, Taiwan
[d]Department of Physics, National Central University, Jungli 32001, Taiwan
[e]Center for Condensed Matter Sciences, National Taiwan University, Taipei 10617, Taiwan
[f]Department of Engineering and System Science, National Tsing Hua University, Hsinchu 30013, Taiwan
† Electronic supplementary information (ESI) available. See DOI: 10.1039/c5nr05988g

This journal is © The Royal Society of Chemistry 2016

Published on 22 December 2015. Downloaded by Academia Sinica - Taipei on 22/01/2016 05:06:09.

region and the strong absorption of GeS spanning in a wide spectral range.

GeS is a p-type semiconductor of an orthorhombic structure with several direct and indirect transitions very close in energy competing for the band gap at ~1.55–1.65 eV, rendering GeS a strong absorber from the visible to near-infrared spectral regions.[19–22] Herein, we report the electrical and optoelectronic characterization of GeS nanosheets, which were exfoliated mechanically from a bulk GeS crystal. Multi-layered GeS nanosheets (~28 nm in thickness) were then used as a conducting channel to fabricate field-effect transistors (FETs). The multi-layered GeS-FETs exhibit remarkably high $R_\lambda \sim 206$ A W^{-1} under illumination of 1.5 μW cm^{-2} at $\lambda = 633$ nm (V_g = 0 V, V_{ds} = 10 V) and possess robust optoelectronic merits to serve as photodetectors of high photocurrent generation. The obtained $R_\lambda \sim 206$ A W^{-1} is excellent in the photocurrent generation as compared with a GeS nanoribbon-based photodetector and the other family members of other group IV–VI photodetectors, such as GeSe and SnS_2 (see ESI Table S1†). Moreover, the multi-layered GeS photodetector exhibits high external quantum efficiency (EQE ~ 4.0×10^4%) and specific detectivity ($D^* \sim 2.35 \times 10^{13}$ Jones). The measured D^* is comparable to the advanced few-layered GaS (~10^{13} Jones)[11] and commercial Si (10^{13} Jones)[23] based photodiodes. Furthermore, the D^* value can be increased by simply tuning the external gate voltage. Light-induced current *vs.* elapsed time (I_{ds}–t) measurements of the multi-layered GeS-FETs reveal the excellent photoresponse time and photoswitching stability of the materials over a long period of operation. These figures-of-merit demonstrate that GeS nanosheets hold great potential for optoelectronic applications, especially for fabricating photodetectors with high photocurrent generation, fast response, and long-term stability.

Results and discussion

The bulk GeS crystals used in this study were grown *via* a chemical vapor transport (CVT) method[24] with the synthetic details being described in the Experimental section. Fig. 1a shows the three-dimensional (3D) crystal structure of GeS, which emphasizes the stacking order and van der Waals interaction among individual sheets in the GeS crystal. The X-ray diffraction (XRD) pattern of the bulk GeS crystal in Fig. 1b confirms that the GeS crystal belongs to the orthorhombic *Pbnm* space group (JCPDS no. 00-051-1168) with lattice constants of a = 4.30 Å, b = 10.47 Å, and c = 3.64 Å. The inset of Fig. 1b presents the selected area electron diffraction (SAED) pattern which exhibits the single-crystallinity of the GeS nanosheets oriented along the [100] direction.[25] In addition, the binding energies of Ge (3d) at 29.6 eV, S ($2p_{3/2}$) at 160.2 eV, and S ($2p_{1/2}$) at 161.4 eV, observed by X-ray photoelectron spectroscopy (XPS) (Fig. 1c), agree well with the earlier report.[26] The crystal morphology and elemental compositions of the GeS crystal, determined by scanning electron microscopy (SEM) and energy dispersive X-ray spectroscopy (EDS), manifest the layered nature of the GeS crystal (Fig. 1d) and the stoichiometric ratio of Ge : S ~ 1 : 1 (see ESI Fig. S1†).

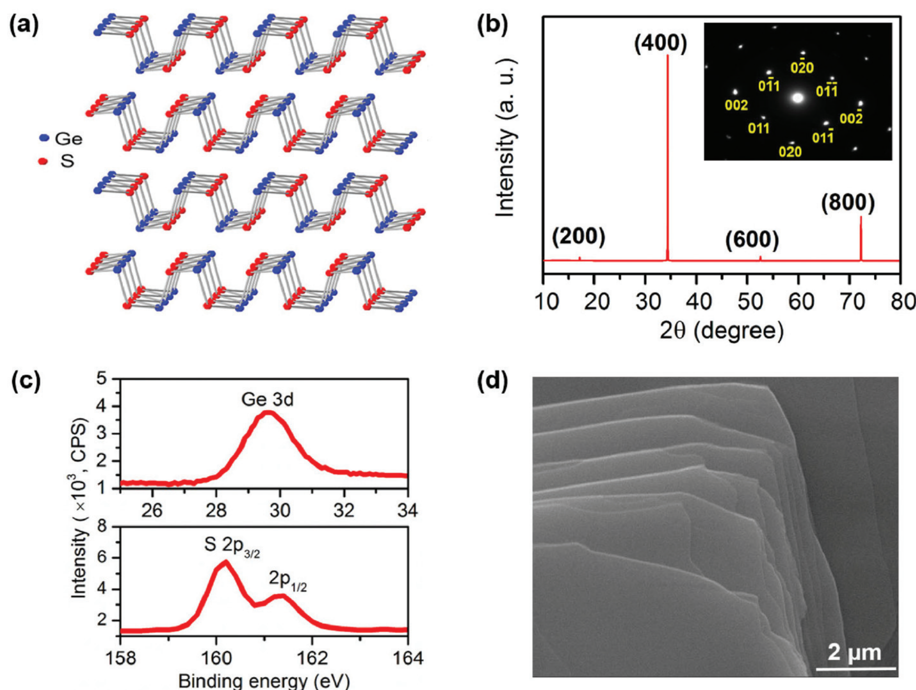

Fig. 1 (a) Crystal structure of GeS. (b) XRD spectrum of the as-synthesized bulk GeS crystal. The inset shows the SAED pattern of GeS nanosheets. (c) Observed XPS spectra of the bulk GeS crystal indicate the binding energies of Ge (3d) at 29.6 eV, S ($2p_{3/2}$) at 160.2 eV, and S ($2p_{1/2}$) at 161.4 eV. (d) SEM image of layered GeS nanosheets.

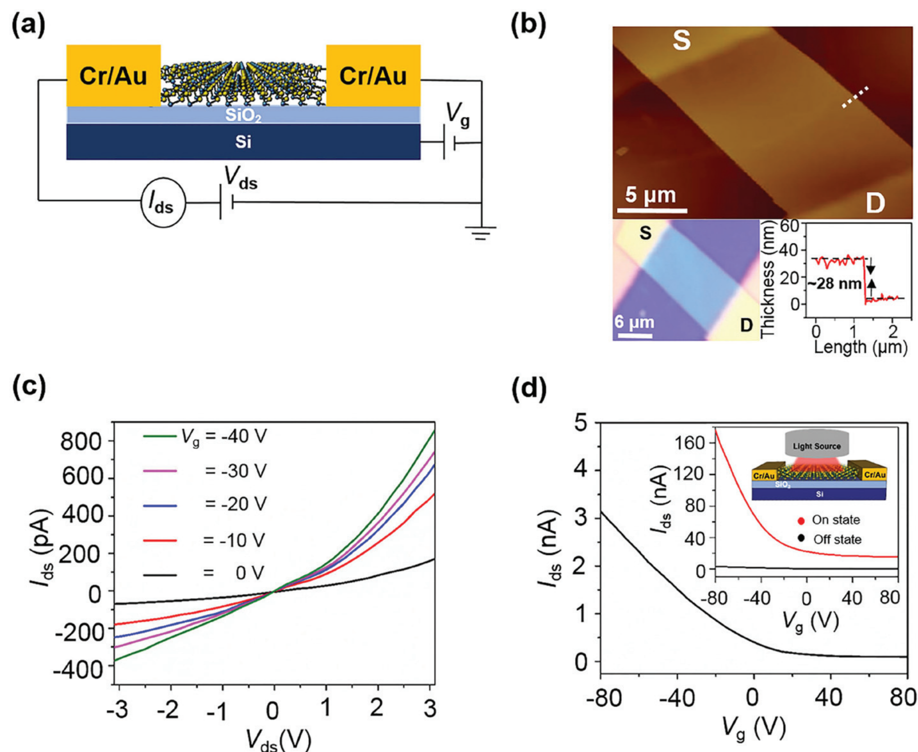

Fig. 2 (a) Illustration of a multi-layered GeS-FET. (b) AFM surface topograph (top panel) and optical image (bottom left panel) of the as-fabricated GeS-FET device. S and D represent the source and drain electrodes, respectively. The thickness of the GeS nanosheets, as scanned along the white dashed line in the top panel, is ~28 nm (bottom right panel). (c) The I_{ds}–V_{ds} characteristic curves of the multi-layered (~28 nm thick) GeS-FET measured at different V_g from 0 to −40 V. (d) The I_{ds}–V_g curve with V_g scanned from 80 to −80 V at V_{ds} = 10 V. The inset shows the transfer curves in the white-light illumination and dark states, in which the upper illustration represents the measurement of a multi-layered GeS-FET under illumination.

Published on 22 December 2015. Downloaded by Academia Sinica - Taipei on 22/01/2016 05:06:09.

Multi-layered GeS-FETs, as illustrated in Fig. 2a, were fabricated following a standard lithographic procedure, where GeS nanosheets on a Si wafer of a 300-nm-thick SiO_2 dielectric layer were electrically connected to Cr/Au (5/70 nm) electrodes. Fig. 2b presents a surface topograph (top panel) and an optical image (bottom left panel) of the as-fabricated multi-layered GeS-FET with the thickness of the GeS nanosheets determined by atomic force microscopy (AFM) to be ~28 nm (bottom right panel), comprising ~50 successive GeS layers. Multi-layered GeS-FET devices fabricated with a semiconductive channel of ~28 nm thick GeS nanosheets were used throughout this study. The source–drain currents *vs.* source–drain voltage (I_{ds}–V_{ds}) of a multi-layered GeS-FET (Fig. 2c) were measured at different gate voltages (V_g = −40–0 V) in a probe station at 10^{-3} Torr and room temperature. The source–drain current *vs.* back-gate voltage (I_{ds}–V_g) curve (Fig. 2d) measured at V_{ds} = 10 V exhibits the p-type behavior of the GeS-FET because of the presence of Ge vacancies in the prepared GeS crystal.[27] The mobility of charge carriers in the GeS-FET can be deduced from $\mu = [L/(WCV_{ds})]\cdot(dI_{ds}/dV_g)$, where L and W are the length and width of the semiconductor channel of the GeS nanosheets, respectively, and C is the capacitance between the channel and the back gate per unit area ($C = \varepsilon_0\varepsilon_r/d$; ε_0 is the vacuum permittivity, ε_r is the relative permittivity, and d is the thickness of the SiO_2 dielectric layer). The field-effect mobility of the device is calculated to be ~1.5×10^{-3} cm^2 V^{-1} s^{-1}; furthermore, the GeS-FET exhibits a high on/off ratio of ~10^5 (see ESI Fig. S2†). The presence of trap/defect states at the interface between the semiconductor channel and the SiO_2 dielectric layer of an FET device plays a dominant role in the charge carrier mobility.[28,29] Reducing the number of such trap/defect states at the interface could substantially improve the device performances.[30,31]

Next, we investigated the photocurrent generation in the GeS-FET by recording the I_{ds}–V_g curves under white-light illumination (shown in the inset of Fig. 2d). The I_{ds}–V_g measurements shown in the inset of Fig. 2d compare the photoresponses of the GeS-FET under illumination and in the dark. Upon illumination, the channel current was observed to increase dramatically relative to the dark state. Because of the excellent photoresponse of the multi-layered GeS-FET to white light, we conducted further photoelectrical studies of this device with various optical intensities. In this work, we carried out all of the photocurrent measurements under monochromatic illumination at 633 nm unless otherwise specified. Fig. 3a presents the I_{ds}–V_{ds} plots of a GeS-FET in the dark and under illumination with different intensities of 1.5, 3.5, 4.5, 15, 35, 45, and 153 μW cm^{-2}, in which the photo-induced

 This journal is © The Royal Society of Chemistry 2016

Published on 22 December 2015. Downloaded by Academia Sinica - Taipei on 22/01/2016 05:06:09.

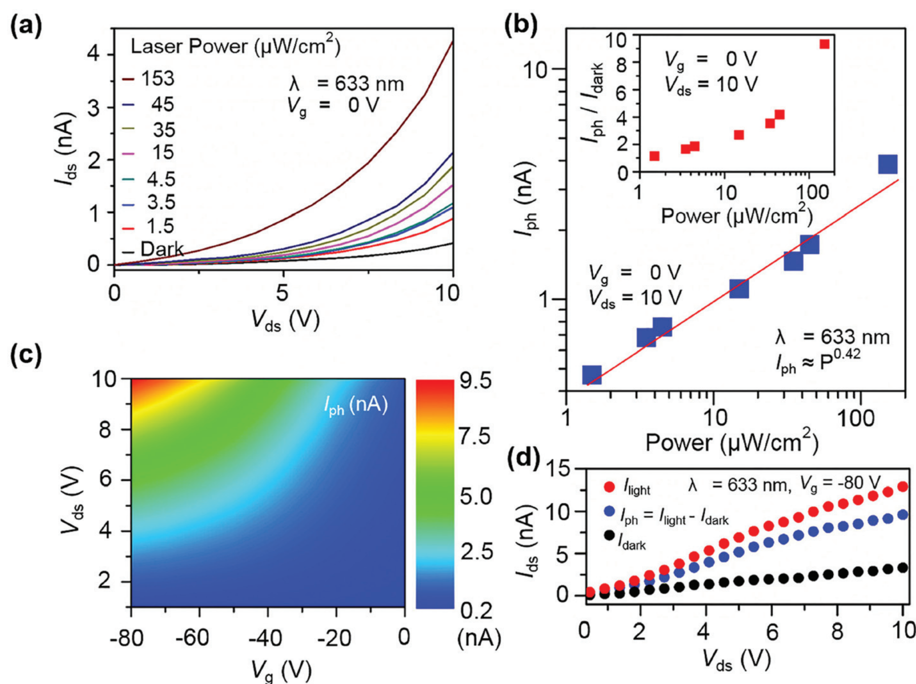

Fig. 3 (a) The I_{ds}–V_{ds} curves of a multi-layered GeS-FET were investigated at V_g = 0 V with 633 nm excitation at laser powers of 1.5, 3.5, 4.5, 15, 35, 45, and 153 μW cm^{-2}. (b) The photocurrent (I_{ph}) is plotted as a function of the incident laser power (P) measured at V_{ds} = 10 V and V_g = 0 V; the data points (blue squares) were collected from (a). A linear fitting (the red solid line) to the experimental data (blue squares) reveals the dependence of the photocurrent on the incident laser power as $I_{ph} \approx P^{0.42}$. The inset shows the photosensitivity (I_{ph}/I_{dark}) as a function of incident laser power measured at V_g = 0 V and V_{ds} = 10 V; the data points (red squares) were collected from (a). (c) Mapping of photocurrent ($I_{ph} = I_{light} - I_{dark}$) as a function of V_g (from 0 to −80 V) and V_{ds} (from 0 to 10 V) under illumination of 1.5 μW cm^{-2} at λ = 633 nm. (d) The I_{ds}–V_{ds} curves of the multi-layered GeS photodetector measured in the illumination and dark states at V_g = −80 V, where the data points were taken from (c).

current gradually increases as the laser power increases. In Fig. 3b, we plot the generated photocurrent (I_{ph}) as a function of the incident laser power (P), where $I_{ph} = I_{light} - I_{dark}$ was calculated by subtracting the I_{ds} obtained in the dark (represented by I_{dark}) from that under illumination (denoted by I_{light}) at V_{ds} = 10 V. The photocurrent increases sublinearly following a power law of $I_{ph} \approx P^{0.42}$, which could be caused by the defects present in GeS and/or the adsorbed molecules/impurities at the GeS–SiO_2/Si interface.[29] The photosensitivity of a device is defined as the ratio of photo-generated current to dark current (*i.e.*, I_{ph}/I_{dark}). A detector of higher photosensitivity exhibits its ability of better noise rejection, where the photocurrent is clearly distinct from the dark current.[32] In the inset of Fig. 3b, we present the increasing photosensitivity (I_{ph}/I_{dark}) as a function of the incident power to manifest the predominant sensitivity of a GeS photodetector to illumination. To gain further insight into the performance of the multi-layered GeS photodetector, the photocurrent ($I_{ph} = I_{light} - I_{dark}$) profile was measured under illumination at different V_{ds} (0–10 V) and V_g (−80–0 V). The mapping in Fig. 3c shows an increase of I_{ph} by raising the negative V_g value with the concomitant rise of V_{ds}. Examining I_{ph} as a function of V_{ds} at a specific V_g = −80 V (Fig. 3d), the multi-layered GeS-FET possesses a low dark current, and the generated I_{ph} is dominated by the photo-generated charge carriers (*i.e.*, photocarriers) upon illumination, making the multi-layered GeS photodetector as a good candidate for optoelectronic applications.

Photoresponsivity (R_λ) is an important parameter to judge the sensitivity of a photodetector under light stimulation. R_λ, which is defined as the photocurrent generated per unit power of the incident light (with wavelength λ) on an active illuminated area, is expressed as $R_\lambda = \Delta I_\lambda/(P_\lambda S) = [et\alpha/(h\nu)]\cdot(\tau_l/\tau_t)$, where ΔI_λ is the generated photocurrent, P_λ is the incident light power, S is the illuminated area, e is the elementary charge, t is the thickness of the channel, α is the absorption coefficient of the channel material at the photon energy of $h\nu$, and τ_l/τ_t is the ratio of the life time of minority carriers (τ_l) to the transit time of majority carriers (τ_t).[13,33] This relationship indicates that both α of the channel material and τ_l/τ_t of the charge carriers are important factors that are responsible for the high photoresponsivity of a photodetector. Fig. 4a shows a 3D perspective of the measured R_λ (0.01–206 A W^{-1}) of a GeS-FET as a function of V_{ds} (0–10 V, V_g = 0 V) and P (153–1.5 μW cm^{-2} at 633 nm). Fig. 4b plots R_λ in response to different incident laser power (P) values at 633 nm with a power law of $R_\lambda \approx P^{-0.6}$. Remarkably, the maximum R_λ of our multi-layered GeS photodetector reaches 206 A W^{-1} at 1.5 μW cm^{-2} (V_{ds} = 10 V and V_g = 0 V). The high R_λ could be accounted for by the strong absorption nature of GeS in a wide spectral range[19–22] together with the fast, effective separation of photo-

Published on 22 December 2015. Downloaded by Academia Sinica - Taipei on 22/01/2016 05:06:09.

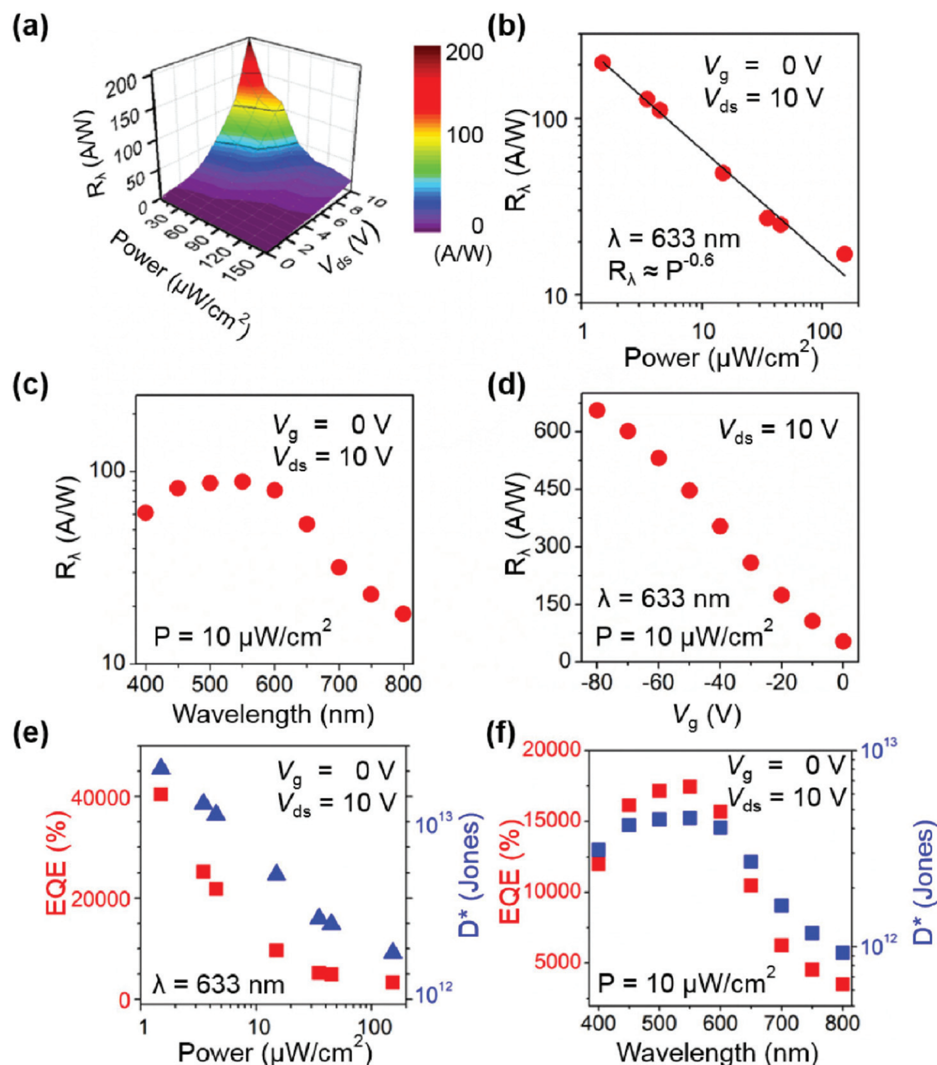

Fig. 4 (a) 3D photoresponsivity map of a multi-layered GeS photodetector. (b) Photo responsivity of the multi-layered GeS photodetector under various laser intensities at 633 nm. The power law of $R_\lambda \approx P^{-0.6}$ was determined from fitting the measured data. The GeS photodetector shows a maximal R_λ of 206 A W^{-1} excited at 1.5 μW cm^{-2}, V_g = 0 V, and V_{ds} = 10 V. (c) The measured R_λ of the multi-layered GeS-FET device with respect to excitation wavelength. (d) R_λ of the multi-layered GeS photodetector as a function of V_g measured at V_{ds} = 10 V and P = 10 μW cm^{-2}. (e) The examined laser power dependences of EQE and D^* for the multi-layered GeS-FET at V_g = 0 V and V_{ds} = 10 V. (f) The EQE and D^* of the multi-layered GeS photodetector were investigated as a function of excitation wavelength at P = 10 μW cm^{-2}, V_g = 0 V, and V_{ds} = 10 V.

carriers in the spatial 2D crystals of GeS nanosheets to defer electron–hole recombination and also by the large τ_l/τ_t, leading to a highly efficient photoresponsive conversion. In this study, we estimated $\tau_l/\tau_t \sim 1.4 \times 10^4$ for our GeS-FET device by calculating the τ_l/τ_t value from the above formula of R_λ with the assistance of computing $eta\alpha/(h\nu)$. Likewise, we also estimated the τ_l/τ_t values of multi-layered SnS_2-, multi-layered GeSe-, and GeS nanoribbon-based FET devices by extracting the available R_λ and $eta\alpha/(h\nu)$ values from reported literature data. These estimated τ_l/τ_t values, together with the channel thicknesses and lengths, of multi-layered GeS-, SnS_2-, and GeSe-FET devices and the GeS nanoribbon-based FET are listed in Table S1† for comparison. The GeS-FET performs substantially better in photoresponsivity as compared with GeS nanoribbon-based (139.9 A W^{-1})[34] and the same group IV–VI family of GeSe- and SnS_2-based photodetectors (see ESI Table S1†). The higher photoresponsivity of GeS nanosheet-based FETs, as compared to 1D GeS nanowire-based FETs, was also reported earlier[22] and can be ascribed to the large surface area of the nanosheets to facilitate the more efficient generation of photo-excited carriers, resulting in higher photocurrent. In order to provide an insight into spectral response of the multi-layered GeS photodetector, we also measured the excitation wavelength dependences of R_λ at 400–800 nm, P = 10 μW cm^{-2}, V_{ds} = 10 V, and V_g = 0 V (Fig. 4c). The R_λ value reaches a maximum of 89 A W^{-1} at $\lambda \sim$ 550 nm and is generally in line with the trends of the observed absorption spectrum (see ESI Fig. S3†) and photoconductivity measurement[35] of a

This journal is © The Royal Society of Chemistry 2016

View Article Online

Published on 22 December 2015. Downloaded by Academia Sinica - Taipei on 22/01/2016 05:06:09.

bulk GeS crystal. Note that R_λ can be further increased by simply tuning the gate voltage (V_g) as shown in Fig. 4d,[13] where the V_g-dependent R_λ was measured at $P = 10\ \mu W\ cm^{-2}$, $V_{ds} = 10$ V, and V_g (−80–0 V). Remarkably, the R_λ increased significantly from 54 to 655 A W^{-1} when V_g was swept from 0 to −80 V.

Next, we determined two other key parameters in photodetection, EQE and D^*, for the multi-layered GeS photodetector. EQE is the measure of the photoconductive gain, which is the number of electrons detected per incident photon (*i.e.*, the photon-to-electron conversion), and can be expressed as EQE = $R_\lambda \cdot [hc/(e\lambda)]$, where R_λ is the photoresponsivity, h is Planck's constant, c is the speed of light, e is the elementary charge, and λ is the incident light wavelength. Based on the relationship of EQE to R_λ, the multi-layered GeS-FET possesses a high EQE of $\sim 4.0 \times 10^4$%, which could be due to both high R_λ and the large surface-to-volume ratio of the 2D layered GeS nanosheets explained as follows. The processes for the photon-to-electron conversion start from the generation of free electron–hole pairs upon photon absorption. The spatial separation of photocarriers in the broad 2D crystal planes of GeS could preclude the electron–hole recombination. The aforementioned trap/defect states, which could be exacerbated further because of the high surface-to-volume ratio of the 2D GeS, were able to capture one type of photo-generated charge carrier while the other type escaped.[36,37] As a result, the escaping photocarrier with prolonged lifetime can make several effective transits in the GeS channel between the electrodes, thus enhancing the photoconductive gain.[38,39]

The D^* value, used to quantify the ability of a photodetector to detect weak optical signals, is defined by $D^* = (S \cdot \Delta f)^{1/2}/\mathrm{NEP}$, where S and Δf are the effective area and electrical bandwidth of the photodetector, respectively, and NEP represents noise equivalent power. The NEP is an indicator of the minimum impinging optical power that a photodetector can distinguish a signal from noise. But, if the photodetector has a low value of NEP, then the above expression can be simplified as $D^* = R_\lambda S^{1/2}/(2eI_{dark})^{1/2}$, where R_λ, S, e, and I_{dark} are the photoresponsivity, effective area, elementary charge, and dark current, respectively.[11,23,40–42] The high $D^* \sim 2.35 \times 10^{13}$ Jones (at $V_g = 0$ and $V_{ds} = 10$ V) obtained for the multi-layered GeS photodetector is due to its low I_{dark} and high R_λ. The obtained D^* is comparable to the recent 2D material-based photodetectors, *e.g.*, GaS ($\sim 10^{13}$ Jones)[11] and In_2Se_3 ($\sim 10^{12}$ Jones)[42] in the visible spectral regions and is close to the advanced commercial Si (10^{13} Jones)- and InGaAs (10^{12-13} Jones)-based photodiodes.[23] Fig. 4e presents the EQE and D^* of a multi-layered GeS photodetector measured with respect to the incident laser power. The excitation wavelength-dependences of EQE and D^* are also presented in Fig. 4f and the D^* *vs.* V_g measurement is shown in Fig. S4 of the ESI.†

Finally, time-resolved measurements were conducted to show the photoresponse and photoswitching stability of the multi-layered GeS photodetector in response to light illumination. The I_{ds}–t plot was recorded by exciting the multi-layered GeS device with a train of on–off illumination at 633 nm. Fig. 5a shows the GeS-FET device in response to a single on–off cycle of illumination ($P = 12.7$ mW cm^{-2}, $V_{ds} = 10$ V, and $V_g = 0$ V), which exhibits a fast rise of current (I_{ds}) under illumination and a sudden drop followed by a much slower relaxation after switching off the laser. While the rising time of the photo-generated signal was determined 7 ± 2 ms from a systematic measurement with several GeS-FET devices, the falling time consists of two components with a fast decay of 9 ± 1 ms

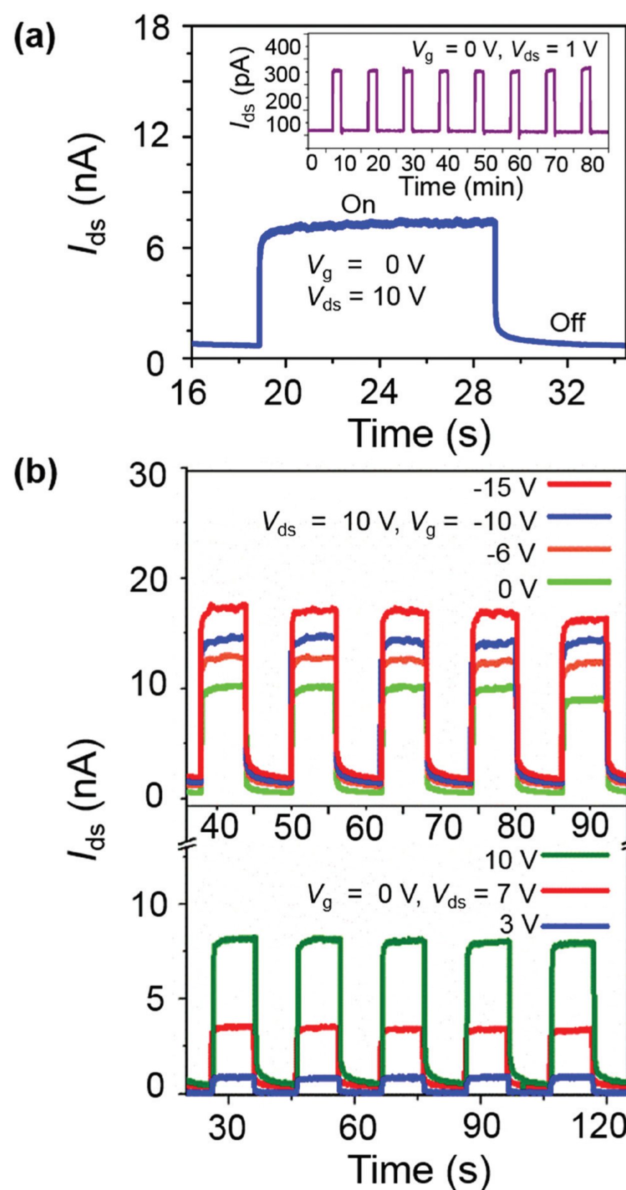

Fig. 5 (a) Time-resolved photoresponse of the multi-layered GeS photodetector was measured in response to a single on–off cycle of illumination at $P = 12.7$ mW cm^{-2} ($\lambda = 633$ nm), $V_g = 0$ V, and $V_{ds} = 10$ V. The inset shows the photoswitching stability of a GeS photodetector in response to a train of pulsed illumination at $P = 12.7$ mW cm^{-2} ($\lambda = 633$ nm), $V_g = 0$ V, and $V_{ds} = 1$ V. (b) Time-resolved photoresponse of the GeS photodetector was examined at various V_g (= 0, −6, −10, and −15 V) and V_{ds} (= 3, 7, and 10 V), respectively.

This journal is © The Royal Society of Chemistry 2016

Published on 22 December 2015. Downloaded by Academia Sinica - Taipei on 22/01/2016 05:06:09.

(corresponding to the earlier 50% decrease) and a slow relaxation of ~2 s (in the latter half of the decline). The response time of the multi-layered GeS photodetector is found to be faster than the recently reported GeS nanoribbon-based photodetector[34] by more than two orders of magnitude and is comparable to those of GaSe-[12] and In_2Se_3-based photodetectors.[42] The relatively long photocarriers lifetime, compared with traditional metal-semiconductor–metal photodetectors,[43] could again be due to the presence of trap/defect states in the GeS photodevice and/or on the surface of the SiO_2/Si substrate (wafer). Such trap/defect states could interrupt the electron–hole recombination, resulting in prolonging the lifetime of photocarriers.[13] In response to consecutive photoswitching, the robustness and stability of our multi-layered GeS photodevice were examined by a train of pulsed illumination over a long period (~90 min) and a long on–off sequence (~100 cycles), as demonstrated by the I_{ds}–t measurements presented in the inset of Fig. 5a and S5 of the ESI,† respectively. The time-resolved photoresponses of the multi-layered GeS photodevice were further tested at different V_g = 0, −6, −10, and −15 V and V_{ds} = 3, 7, and 10 V (shown in Fig. 5b), where the I_{ds} increases with the increasing amplitude of V_g or V_{ds}. These sustainable rise times and reproducible on–off shapes clearly demonstrate the device robustness, reproducible response, and switching stability of the multi-layered GeS photodetector.

Conclusion

In summary, single-crystalline GeS crystals were synthesized *via* a CVT method. High-quality multi-layered GeS nanosheets were obtained from a bulk GeS crystal *via* adhesive tape exfoliation. Multi-layered GeS-FET devices were fabricated following a standard lithographic procedure. The optoelectronic properties of the multi-layered GeS-FETs at room temperature were explored to render a very high $R_\lambda \sim 206$ A W^{-1} (at λ = 633 nm, P = 1.5 μW cm^{-2}, V_g = 0 V, and V_{ds} = 10 V) and EQE ~ 4.0×10^4%, both of which are excellent among the recently reported 2D crystal-based photodetectors. Moreover, the value of $D^* \sim 2.35 \times 10^{13}$ Jones of the multi-layered GeS-FETs (measured at V_g = 0 V and V_{ds} = 10 V) is comparable to those of the advanced commercial Si- and InGaAs-based photodiodes. Finally, the multi-layered GeS photodetectors exhibit device robustness, photoswitching stability, and long-term durability. These extraordinary photoresponses allow the multi-layered GeS photodetectors to occupy a significant place in future optoelectronic applications.

Experimental section

Crystal growth

GeS crystals were grown from the CVT reaction in a three-zone horizontal furnace with the experimental conditions listed in Table 1. The furnace was constructed by using a quartz tube closed at one end with dimensions of 100 cm in length and 12 cm/10 cm in outer/inner diameter. For the crystal growth, high-quality quartz ampoules of 32 cm in length and 2 cm/1.8 cm in outer/inner diameter were filled with ~10 g samples containing the stoichiometric proportion (1 : 1) of Ge (99.999% purity) and S (99.999% purity) and were sealed at 10^{-5} Torr. After the sealed ampoules were placed in the three-zone horizontal furnace, the reaction and growth zones were slowly heated and later maintained at specific temperatures during the growth period. The experimental conditions for the growth of GeS single crystals are listed in Table 1.[44]

Table 1 The experimental conditions for the growth of GeS single crystals

Synthesized crystal	Reaction/growth temperature		Growth period	Dimensions of the as-grown crystal
	Reaction zone	Growth zone		
GeS	Zone 1 at 873 K Zone 2 at 850 K	Zone 3 at 800 K	100 h	7.5 × 6.5 × 0.5 mm^3

Mechanical exfoliation

The as-synthesized single-crystal GeS flakes were exfoliated into multi-layered GeS nanosheets using a simple mechanical exfoliation method. Briefly, the bulk GeS crystal was placed on an adhesive tape, and the GeS layers were peeled off by slight rubbing and slicing. The rubbing–slicing process was repeated several times before transferring the GeS nanosheets to a Si wafer containing a 300 nm thick SiO_2 dielectric layer. The transferred GeS nanosheets on the Si wafer were inspected using an optical microscope (Olympus, BX 51M) equipped with a charge-coupled device (CCD) camera (Leica, DFC495). The thickness of the GeS nanosheets was estimated from their different interference colors in the optical image and was later determined from atomic force microscopy (AFM) (Veeco, Bio-Scope SZ) scans.

Device fabrication

For the device fabrication of the multi-layered GeS-FETs, a transmission electron microscope (TEM) copper grid was mounted on the as-exfoliated GeS nanosheets on a Si wafer using a homemade micro-manipulator. The TEM grid acted as a shadow mask for the deposition of metallic electrodes (5 nm Cr/70 nm Au) in a thermal evaporator to fabricate the multi-layered GeS-FETs.

Optoelectronic characterization

The optoelectronic properties of the bulk GeS crystals, the as-exfoliated multi-layered GeS nanosheets, and the as-fabricated multi-layered GeS-FETs were characterized using various techniques. The lattice constant and crystal structure were examined with an X-ray diffractometer (X'Pert PRO-PANalytical, CuKα radiation). The morphology and crystallinity were investi-

 This journal is © The Royal Society of Chemistry 2016

Published on 22 December 2015. Downloaded by Academia Sinica - Taipei on 22/01/2016 05:06:09.

gated by scanning electron microscopy (SEM) (FEI, Nova 200) and transmission electron microscopy (TEM) (JEOL, JEM-2100F). The electrical and optical parameters of the multi-layered GeS devices were measured at room temperature in a probe station (Lakeshore, TTPX) at 10^{-3} Torr equipped with a source meter (Keithley, 2636A) and an optical system, including a He–Ne laser (JDS Uniphase, Novette 1507), a power meter (Ophir, Nova II), an optical beam shutter (Thorlabs, SH1), a xenon lamp (Newport, 66921), and a monochromator (Acton, SpectraPro-500). The photoresponse time measurements were conducted *via* a Semiconductor Devices Parameter Analyzer (Agilent Technologies, B1500 A).

Author contribution statement

R. K. U. designed the experiments. R. K. U. and Y. Y. L. carried out electrical and optical measurements. C. J. K. performed spectral experiments with wavelength dependence. R. K. U. and S. R. T. fabricated field-effect transistor devices. R. S. and F. C. C. grew GeS crystals. K. M. B., A. A., K. Y., and R. J. M. assisted the experiments of electrical and optoelectronic characterization. C. R. L. conducted real-time photoresponsive measurements. R. K. U. wrote the manuscript. Y. T. C. is the corresponding author in charge of the project design, experimental data analysis, and manuscript writing.

Acknowledgements

This work was partially supported by the Ministry of Science and Technology of Taiwan under Grant No. 103-2627-M-002-009, 103-2113-M-002-014-MY3, and 102-2119-M-002-004 and by Academia Sinica under AC Nano Program_2014. We thank Prof. Chun-hsien Chen for lending us a Semiconductor Devices Parameter Analyzer for photoresponse time measurements. Technical support from NanoCore, the Core Facilities for Nanoscience and Nanotechnology at Academia Sinica, is also acknowledged.

References

1 F. Xia, T. Mueller, Y.-m. Lin, A. Valdes-Garcia and P. Avouris, *Nat. Nanotechnol.*, 2009, **4**, 839.
2 Z. Sun, T. Hasan, F. Torrisi, D. Popa, G. Privitera, F. Wang, F. Bonaccorso, D. M. Basko and A. C. Ferrari, *ACS Nano*, 2010, **4**, 803.
3 S. Bae, H. Kim, Y. Lee, X. Xu, J.-S. Park, Y. Zheng, J. Balakrishnan, T. Lei, H. Ri Kim, Y. I. Song, Y.-J. Kim, K. S. Kim, B. Ozyilmaz, J.-H. Ahn, B. H. Hong and S. Iijima, *Nat. Nanotechnol.*, 2010, **5**, 574.
4 M. Liu, X. Yin, E. Ulin-Avila, B. Geng, T. Zentgraf, L. Ju, F. Wang and X. Zhang, *Nature*, 2011, **474**, 64.
5 S. Z. Butler, S. M. Hollen, L. Cao, Y. Cui, J. A. Gupta, H. R. Gutiérrez, T. F. Heinz, S. S. Hong, J. Huang, A. F. Ismach, E. Johnston-Halperin, M. Kuno, V. V. Plashnitsa, R. D. Robinson, R. S. Ruoff, S. Salahuddin, J. Shan, L. Shi, M. G. Spencer, M. Terrones, W. Windl and J. E. Goldberger, *ACS Nano*, 2013, **7**, 2898.
6 J. A. Rogers, M. G. Lagally and R. G. Nuzzo, *Nature*, 2011, **477**, 45.
7 B. Radisavljevic, A. Radenovic, J. Brivio, V. Giacometti and A. Kis, *Nat. Nanotechnol.*, 2011, **6**, 147.
8 Y. Shi, C. Hua, B. Li, X. Fang, C. Yao, Y. Zhang, Y.-S. Hu, Z. Wang, L. Chen, D. Zhao and G. D. Stucky, *Adv. Funct. Mater.*, 2013, **23**, 1832.
9 D. Ovchinnikov, A. Allain, Y.-S. Huang, D. Dumcenco and A. Kis, *ACS Nano*, 2014, **8**, 8174.
10 Y.-F. Lin, Y. Xu, S.-T. Wang, S.-L. Li, M. Yamamoto, A. Aparecido-Ferreira, W. Li, H. Sun, S. Nakaharai, W.-B. Jian, K. Ueno and K. Tsukagoshi, *Adv. Mater.*, 2014, **26**, 3263.
11 P. Hu, L. Wang, M. Yoon, J. Zhang, W. Feng, X. Wang, Z. Wen, J. C. Idrobo, Y. Miyamoto, D. B. Geohegan and K. Xiao, *Nano Lett.*, 2013, **13**, 1649.
12 P. Hu, Z. Wen, L. Wang, P. Tan and K. Xiao, *ACS Nano*, 2012, **6**, 5988.
13 S. R. Tamalampudi, Y.-Y. Lu, R. Kumar, U. R. Sankar, C.-D. Liao, K. Moorthy, B. C.-H. Cheng, F. C. Chou and Y.-T. Chen, *Nano Lett.*, 2014, **14**, 2800.
14 C. Li, L. Huang, G. P. Snigdha, Y. Yu and L. Cao, *ACS Nano*, 2012, **6**, 8868.
15 D.-J. Xue, J. Tan, J.-S. Hu, W. Hu, Y.-G. Guo and L.-J. Wan, *Adv. Mater.*, 2012, **24**, 4528.
16 Z. Deng, D. Cao, J. He, S. Lin, S. M. Lindsay and Y. Liu, *ACS Nano*, 2012, **6**, 6197.
17 L. Li, Z. Chen, Y. Hu, X. Wang, T. Zhang, W. Chen and Q. Wang, *J. Am. Chem. Soc.*, 2013, **135**, 1213.
18 B. Mukherjee, Y. Cai, H. R. Tan, Y. P. Feng, E. S. Tok and C. H. Sow, *ACS Appl. Mater. Interfaces*, 2013, **5**, 9594.
19 L. Makinistian and E. A. Albanesi, *Phys. Rev. B: Condens. Matter*, 2006, **74**, 045206.
20 T. Grandke and L. Ley, *Phys. Rev. B: Solid State*, 1977, **16**, 832.
21 J. D. Wiley, A. Breitschwerdt and E. Schönherr, *Solid State Commun.*, 1975, **17**, 355.
22 L. Shi and Y. Dai, *J. Appl. Crystallogr.*, 2014, **47**, 527.
23 X. Gong, M. Tong, Y. Xia, W. Cai, J. S. Moon, Y. Cao, G. Yu, C.-L. Shieh, B. Nilsson and A. J. Heeger, *Science*, 2009, **325**, 1665.
24 O. V. Yazyevand and A. Kis, *Mater. Today*, 2015, **18**, 20.
25 D. D. Vaughn Ii, R. J. Patel, M. A. Hickner and R. E. Schaak, *J. Am. Chem. Soc.*, 2010, **132**, 15170.
26 S. Murugesan, P. Kearns and K. J. Stevenson, *Langmuir*, 2012, **28**, 5513.
27 D. I. Bletskan, I. I. Madyar, S. V. Mikulaninets and M. Y. Sichka, *Inorg. Mater.*, 2000, **36**, 544.
28 Z. Yin, H. Li, H. Li, L. Jiang, Y. Shi, Y. Sun, G. Lu, Q. Zhang, X. Chen and H. Zhang, *ACS Nano*, 2012, **6**, 74.
29 S. Ghatak, A. N. Pal and A. Ghosh, *ACS Nano*, 2011, **5**, 7707.

Published on 22 December 2015. Downloaded by Academia Sinica - Taipei on 22/01/2016 05:06:09.

30 W. Feng, W. Zheng, W. Cao and P. Hu, *Adv. Mater.*, 2014, **26**, 6587.
31 S. Sucharitakul, N. J. Goble, U. R. Kumar, R. Sankar, Z. A. Bogorad, F.-C. Chou, Y.-T. Chen and X. P. A. Gao, *Nano Lett.*, 2015, **15**, 3815.
32 J. D. Hwang, Y. H. Chen, C. Y. Kung and J. C. Liu, *IEEE Trans. Electron Devices*, 2007, **54**, 2386.
33 G. W. Mudd, S. A. Svatek, L. Hague, O. Makarovsky, Z. R. Kudrynskyi, C. J. Mellor, P. H. Beton, L. Eaves, K. S. Novoselov, Z. D. Kovalyuk, E. E. Vdovin, A. J. Marsden, N. R. Wilson and A. Patane, *Adv. Mater.*, 2015, **27**, 3760.
34 C. Lan, C. Li, Y. Yin, H. Guo and S. Wang, *J. Mater. Chem. C*, 2015, **3**, 8074.
35 A. M. Elkorashy, *J. Phys.: Condens. Matter*, 1990, **2**, 6195.
36 M. M. Furchi, D. K. Polyushkin, A. Pospischil and T. Mueller, *Nano Lett.*, 2014, **14**, 6165.
37 A. R. Klots, A. K. M. Newaz, B. Wang, D. Prasai, H. Krzyzanowska, J. Lin, D. Caudel, N. J. Ghimire, J. Yan, B. L. Ivanov, K. A. Velizhanin, A. Burger, D. G. Mandrus, N. H. Tolk, S. T. Pantelides and K. I. Bolotin, *Sci. Rep.*, 2014, **4**, 6608.
38 G. Konstantatos, M. Badioli, L. Gaudreau, J. Osmond, M. Bernechea, F. P. G. de Arquer, F. Gatti and F. H. L. Koppens, *Nat. Nanotechnol.*, 2012, **7**, 363.
39 X. Li, J. E. Carey, J. W. Sickler, M. U. Pralle, C. Palsule and C. J. Vineis, *Opt. Express*, 2012, **20**, 5518.
40 M. Buscema, J. O. Island, D. J. Groenendijk, S. I. Blanter, G. A. Steele, H. S. J. van der Zant and A. C. Gomez, *Chem. Soc. Rev.*, 2015, **44**, 3691.
41 G. Su, V. G. Hadjiev, P. E. Loya, J. Zhang, S. Lei, S. Maharjan, P. Dong, P. M. Ajayan, J. Lou and H. Peng, *Nano Lett.*, 2015, **15**, 506.
42 R. B. J. Gedrim, M. Shanmugam, N. Jain, C. A. Durcan, M. T. Murphy, T. M. Murray, R. J. Matyi, R. L. Moore and B. Yu, *ACS Nano*, 2014, **8**, 514.
43 M. Y. Liu, E. Chen and S. Y. Chou, *Appl. Phys. Lett.*, 1994, **65**, 887.
44 G. K. Solanki, D. B. Patel, S. Unadkat and M. K. Agarwal, *Pramana*, 2010, **74**, 813.

 This journal is © The Royal Society of Chemistry 2016